Supplement of Atmos. Chem. Phys., 22, 4929–4949, 2022
https://doi.org/10.5194/acp-22-4929-2022-supplement

Atmospheric Chemistry and Physics
Open Access
EGU

Supplement of

Direct measurements of ozone response to emissions perturbations in California

Shenglun Wu et al.

Correspondence to: Michael J. Kleeman (mjkleeman@ucdavis.edu)

1. Configuration of transportable smog chamber system.

The distribution of lights was chosen (shown in Figure S1) to achieve equal UV intensity for each chamber in this geometric configuration. Multiple light configurations were tested with UV measurements at each chamber. The configuration summarized in Figure S1 achieved the most uniform distribution of UV among the chambers. The consistency of O_3 formation in all chambers initialized with the same composition confirms that the light distribution produces the same photolysis rates in each chamber. Moreover, the chamber named bag1,2,3 in the consistency test only represent the position of chamber in the system. The actual chambers were rotated during the consistency checks to verify that the equivalent O_3 formation across chambers was not caused by compensating errors.

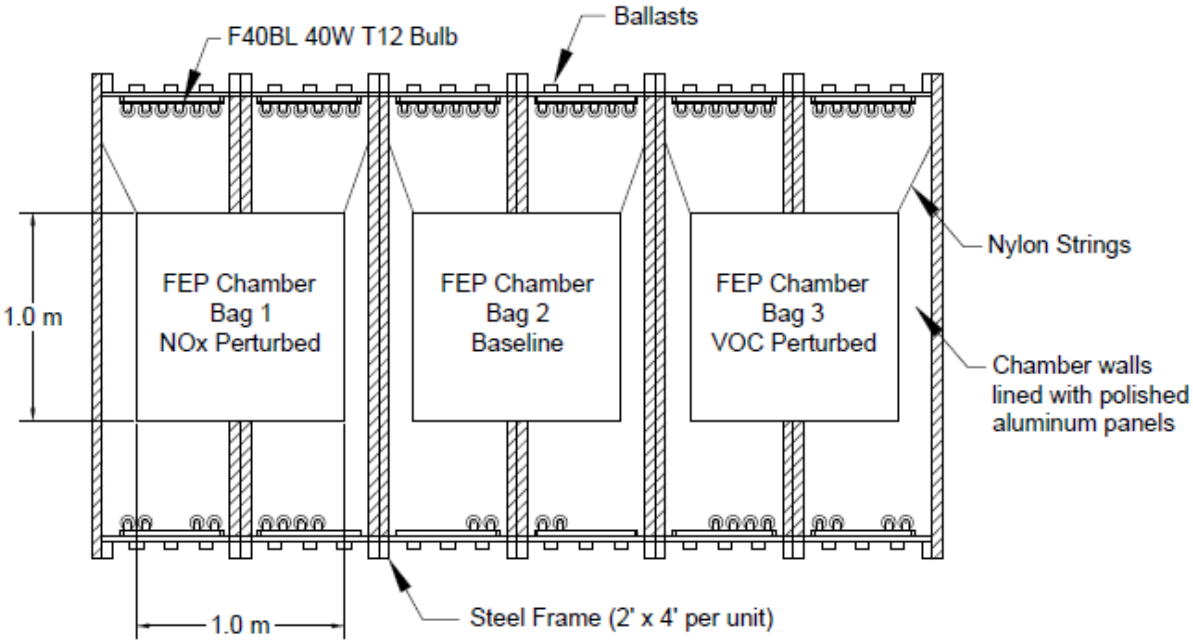

Figure S1. Cross-sectional view of the transportable smog chamber system

2. Consistency of O_3 formation in smog chambers

A t test applied to final O_3 concentration in 3 chambers has p value < 0.03, illustrates the consistency of O_3 formation in 3 chambers.

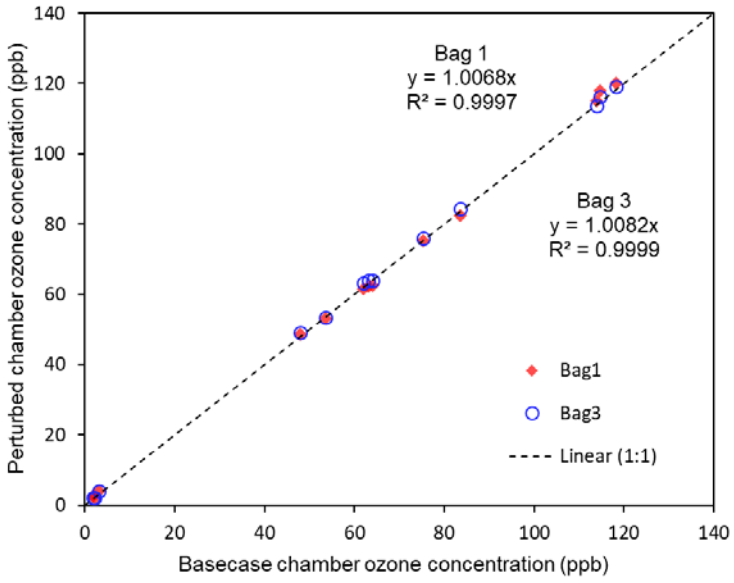

Figure S2. Consistency check of three 1 m^3 FEP bags using equal NO_x-VOC mixture. Points near the origin were measured with zero air. The equation and R^2 shows the linear regression results of O_3 concentration in perturbed chamber to basecase chamber. The 95% confidence intervals (CI) of regression coefficient are (0.996, 1.017) for bag 1, and (1.002, 1.013) for bag 3.

3. Ambient and chamber O_3 formation comparison

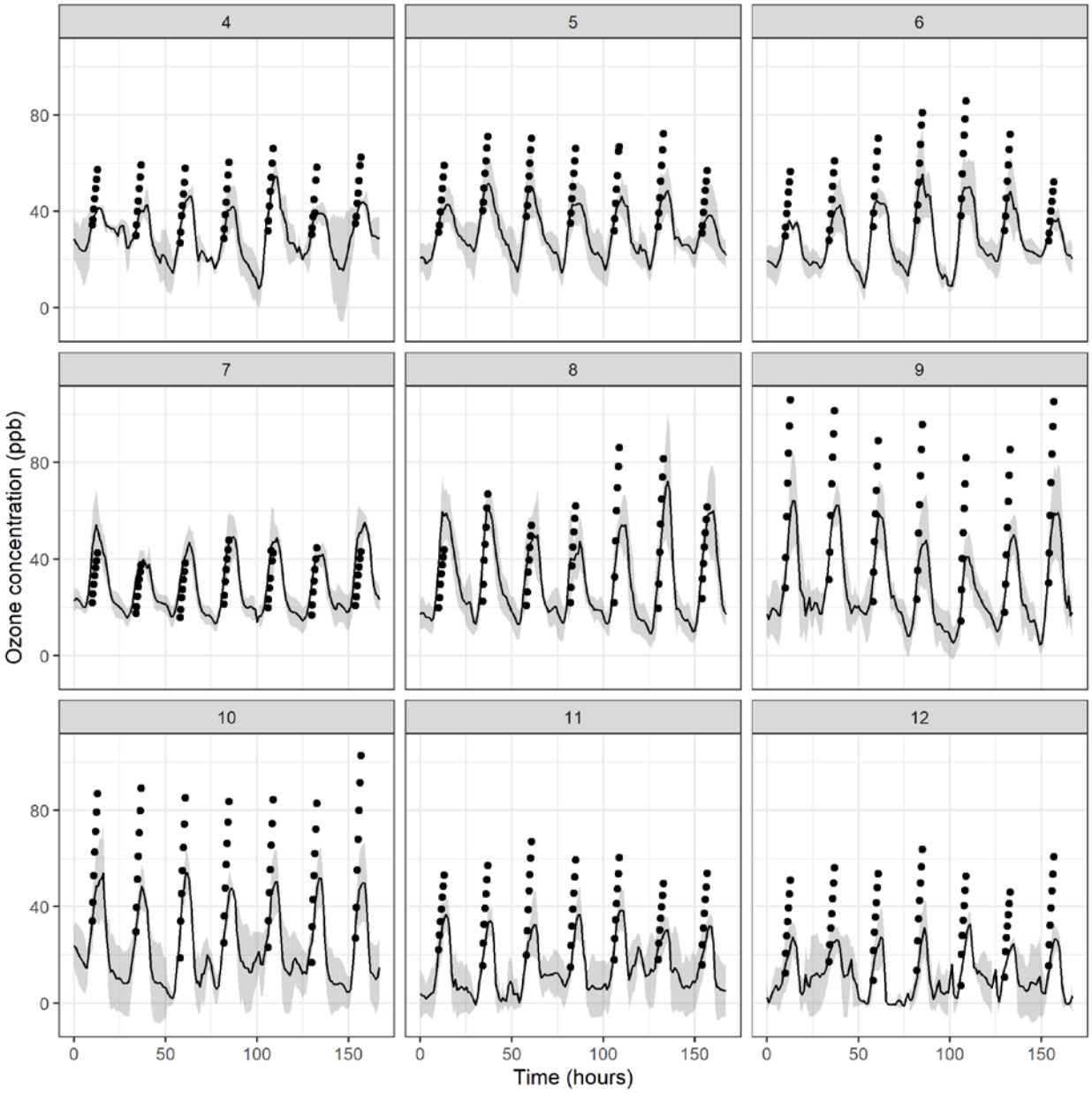

Figure S3. Weekly averaged Ambient (solid line) vs. Chamber (solid circles) O_3 concentrations measured in Sacramento for each month from April to December, 2020. The shaded area indicates one standard deviation of the ambient O_3 concentration. Chambers were filled over a ~2hr period followed by a 30 min measurement period before UV lights were turned on. Hour is relative to the start of the experiment.

4. CO*Biogenic calculation

Temperature and relative humidity-induced enhancement factor for isoprene emissions

$$T = \frac{\exp[T_1(T_L - T_s)/RT_LT_S]}{1 + \exp[T_2(T_L - T_3)/RT_LT_S]}$$

Where T_L is the ambient temperature (kelvins), T_S is the normalizing temperature (301 k), R is the gas constant (8.314 $J\ K^{-1}mol^{-1}$), and T_1 (= 95100 $J\ mol^{-1}$), T_2 (= 231000 $J\ mol^{-1}$), T_3 (= 311.83 k) are empirical coefficient.

$$H = RH \cdot H_1 + H_2$$

Where RH is relative humidity (%) and H_1 (=0.00236) and H_2 (=0.8495) are empirical coefficients.

$$CO * Biogenic = [CO] \times T \times H$$

Where [CO] is CO concentration (ppb) measured in the nearby monitoring station.

5. VOC reactivity (VOCR) and CO*Biogenic correlation

Figure S4 shows the correlation between the sum of species measured in the PAMS network multiplied by their O_3 formation potential (= VOCR) vs. candidate surrogate measures of VOC reactivity (= CO and CO*biogenic). The p-value in each panel quantifies the probability that the surrogate has zero correlation with VOCR. The R-value in each panel quantifies the amount variation about the mean value of VOCR that is explained by the surrogate. CO*biogenic explains 36% of the VOCR variability about the mean VOCR value, while CO alone explains 15% of the VOCR variability about the mean VOCR value. CO*biogenic is therefore selected as the preferred (but not perfect) surrogate for VOC concentrations in the current study.

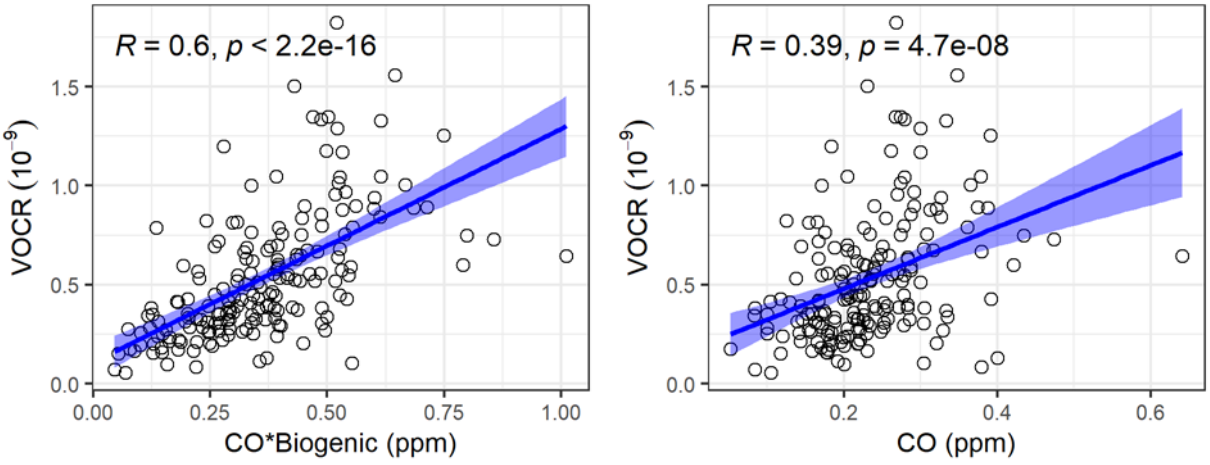

Figure S4. Scatter plot of VOC reactivity vs CO concentration (right) and CO*Biogenic (left) in Sacramento during the years 2010-2019. The shaded area shows the 95% confidence interval of the mean response of the predicted value. The CO, VOC, temperature, and RH data are all from standard monitoring site at Sacramento-Del Paso Manor. Data source: https://aqs.epa.gov/aqsweb/airdata/download_files.html#Raw

6. Location of chamber measurement site in Sacramento

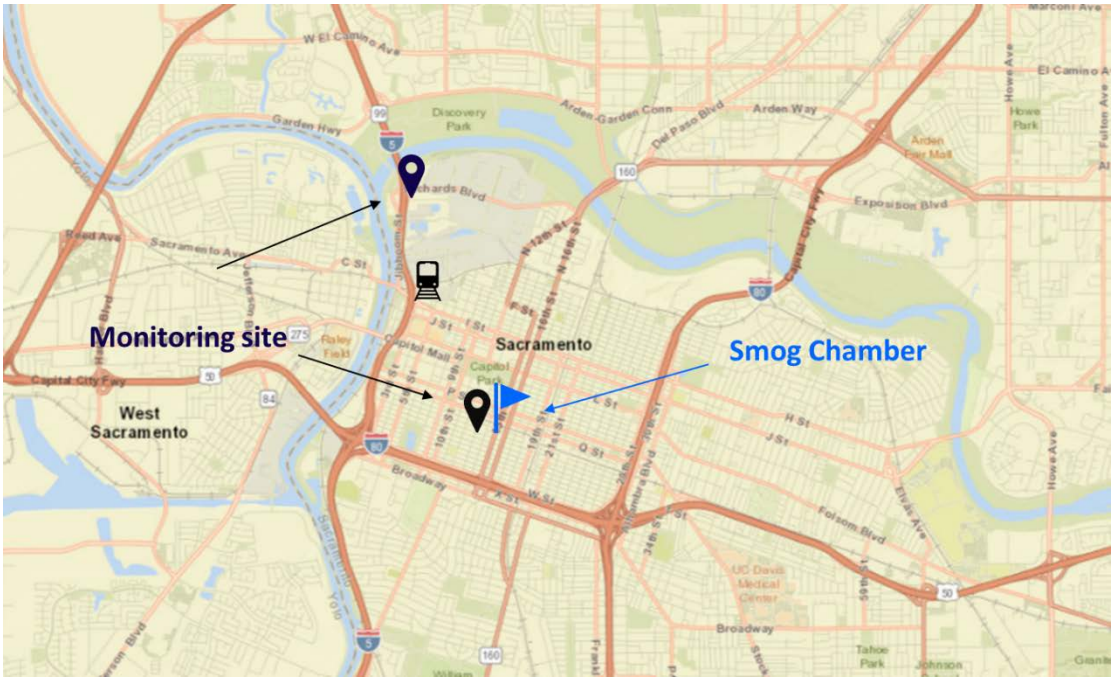

70 **Figure S5. Map shows the location of the sampling site in Sacramento and surrounding facilities. Powered by ESRI. The North CARB monitoring site (Sacramento - Bercut Drive) collects CO concentration used to calculate CO*Biogenic, the south CARB monitoring site (Sacramento-T Street) collects O_3, NO_x concentration used as a quality check data source to the chamber measurement.**

75

7. O_3 sensitivity measurement calculation

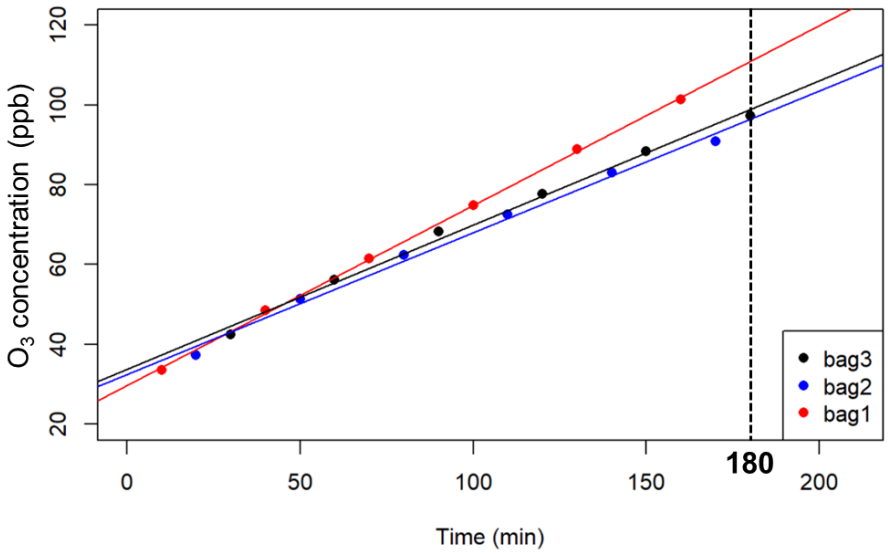

Figure S6. O_3 concentration in 3 chambers under the UV exposure during a typical chamber experiment on August 16, 2020 in Sacramento. Lines shows the linear regression result of O_3 concentration under UV exposure in each chamber.

Figure S6 shows an example of the time series of chamber O_3 concentration under the UV exposure. The time in x-axis reflects the UV exposure duration time in the chamber. Each dot is 10-min averaged O_3 concentration corrected by O_3 wall loss rate. Dots with different colors correspond to different chambers. Linear regression was applied to O_3 concentration in each chamber shown as solid lines. The projected O_3 concentration at the end of the 180-min UV exposure time was calculated based on the regression results (hereafter referred to as $3hr\ O_3^{Bag\ 1}$, $3hr\ O_3^{Bag\ 2}$, and $3hr\ O_3^{Bag\ 3}$). The measured sensitivities $\Delta O_3^{+NO_x}$, and ΔO_3^{+VOC} were calculated using the equation below:

$$\Delta O_3^{+NO_x} = 3hr\ O_3^{Bag\ 2} - 3hr\ O_3^{Bag\ 1}$$

$$\Delta O_3^{+VOC} = 3hr\ O_3^{Bag\ 3} - 3hr\ O_3^{Bag\ 1}$$

8. Comparison between wildfire days and non-wildfire days in TROPOMI data

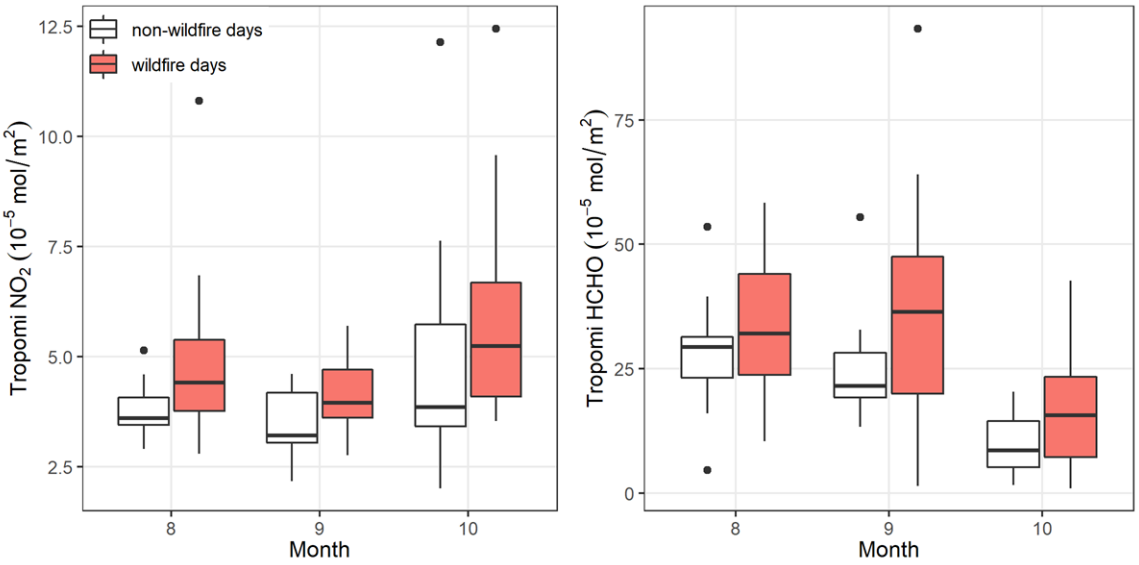

Figure S7. Monthly box and whisker plot of TROPOMI HCHO and NO_2 in wildfire days (solid box) and non-wildfire days (open box) from August to October, 2020. TROPOMI HCHO and NO_2 is in the 5km radii buffer of the chamber measurement site in Sacramento.

9. Chamber and satellite O_3 sensitivity correlation

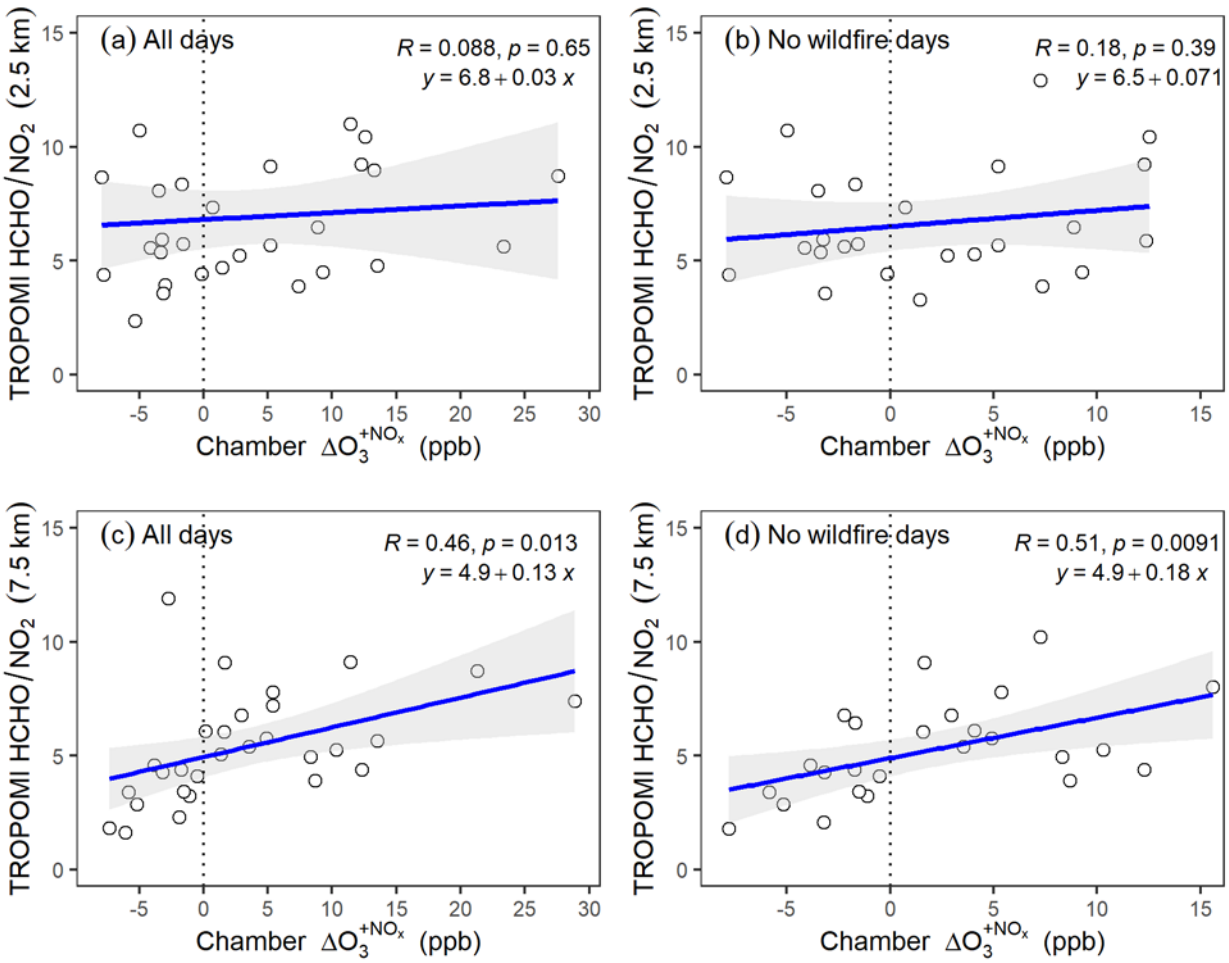

Figure S8. Correlation between weekly averaged TROPOMI satellite HCHO/NO_2 at other two circular buffers (2.5 km (top) and 7.5 km (bottom)) and the weekly averaged chamber $\Delta O_3^{+NO_x}$ from ground-based measurement. The shaded area shows the 95% confidence interval of the mean response of the predicted value.

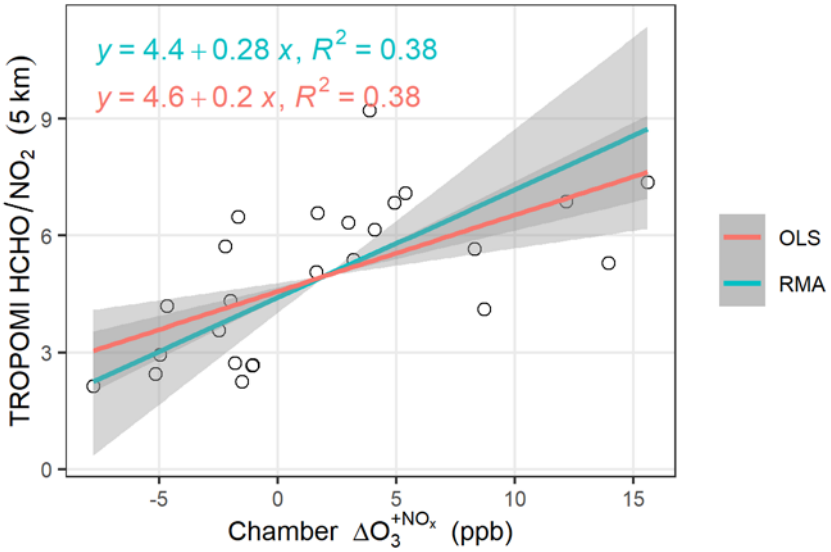

Figure S9. Correlation between weekly averaged TROPOMI HCHO/NO_2 at 5 km circular buffers and the weekly averaged $\Delta O_3^{+NO_x}$ from ground-based measurement during non-wildfire days. The shaded area shows the 95% confidence interval of the mean response of the predicted value. Red regression line generated using ordinary least squares regression. Green regression line generated using reduced major axis regression.

10. Monthly variance of TROPOMI HCHO/NO2 in California

Table S1. Monthly averaged TROPOMI satellite HCHO/NO2 for all air basins in California

Air Basin	N	Feb	Mar	Apr	May	June	July	Aug	Sept	Oct
Northeast Plateau	1701	4.7 (1.9)	3.5 (1.3)	3.4 (1.2)	5.7 (1.2)	9.8 (1.5)	12.4 (2.4)	10.9 (2.2)	11.0 (1.7)	6.8 (0.9)
North Coast	1349	5.0 (1.6)	4.1 (1.1)	4.1 (1.5)	5.2 (1.1)	9.2 (1.7)	12.6 (2.8)	11.5 (2.2)	9.4 (2.7)	6.5 (1.1)
Sacramento	1643	3.9 (1.6)	3.2 (1.1)	3.4 (1.1)	4.7 (1.2)	8.8 (2.0)	11.3 (3.3)	9.8 (2.7)	10.7 (2.2)	5.9 (1.5)
Mountain Counties	1329	3.6 (1.4)	3.5 (1.4)	3.3 (1.3)	4.5 (0.9)	9.9 (1.7)	11.9 (2.3)	9.8 (1.8)	10.8 (2.4)	7.0 (1.7)
Lake County	144	4.5 (1.1)	4.0 (1.2)	4.5 (1.1)	5.0 (1.0)	10.2 (0.8)	12.1 (1.4)	10.3 (2.0)	10.3 (2.2)	5.9 (0.7)
Lake Tahoe	40	2.4 (0.9)	2.8 (1.7)	2.6 (1.1)	3.5 (1.0)	9.0 (1.2)	11.2 (1.3)	8.9 (0.9)	11.7 (0.9)	6.2 (0.7)
Great Basin Valleys	1492	3.4 (1.2)	2.7 (1.2)	3.3 (1.4)	5.0 (1.0)	10.2 (1.7)	10.6 (2.6)	8.3 (1.9)	9.9 (2.2)	7.7 (1.7)
San Francisco Bay	583	1.8 (0.9)	2.4 (0.8)	2.6 (0.9)	3.6 (0.8)	6.2 (1.5)	6.5 (1.6)	6.0 (1.5)	7.4 (1.6)	3.8 (1.1)
San Joaquin Valley	2473	2.6 (1.4)	2.6 (1.3)	3.3 (1.4)	4.3 (1.2)	8.2 (3.4)	8.7 (3.4)	7.5 (2.1)	7.7 (1.6)	6.4 (2.2)
North Central Coast	542	2.8 (0.7)	2.9 (1.0)	3.7 (1.0)	4.9 (0.8)	7.4 (1.1)	8.4 (1.2)	7.4 (1.1)	8.2 (1.2)	5.6 (1.2)
Mojave Desert	2766	2.6 (0.6)	2.6 (0.7)	3.7 (0.9)	4.5 (0.7)	7.8 (1.2)	7.7 (1.3)	6.8 (1.2)	7.2 (1.2)	5.3 (1.0)
South Central Coast	791	2.7 (0.7)	2.6 (0.9)	3.9 (0.9)	5.2 (0.7)	8.8 (1.2)	9.4 (1.4)	8.5 (1.1)	9.6 (1.3)	6.7 (1.2)
South Coast	689	1.1 (0.6)	1.5 (0.7)	2.5 (0.8)	3.4 (1.1)	5.1 (1.9)	5.1 (2.1)	4.5 (1.6)	4.2 (1.9)	3.0 (1.5)
Salton Sea	663	2.5 (0.6)	3.1 (0.6)	3.9 (0.6)	4.8 (0.6)	7.2 (1.0)	7.7 (1.2)	7.1 (1.2)	6.5 (1.1)	4.8 (0.9)
San Diego County	429	2.1 (0.9)	2.4 (0.8)	3.3 (0.8)	4.5 (0.9)	7.4 (1.6)	7.5 (1.9)	7.4 (1.6)	6.9 (1.7)	4.8 (1.5)

Note: Mean (SD) of TROPOMI ($HCHO/NO_2$) shown.

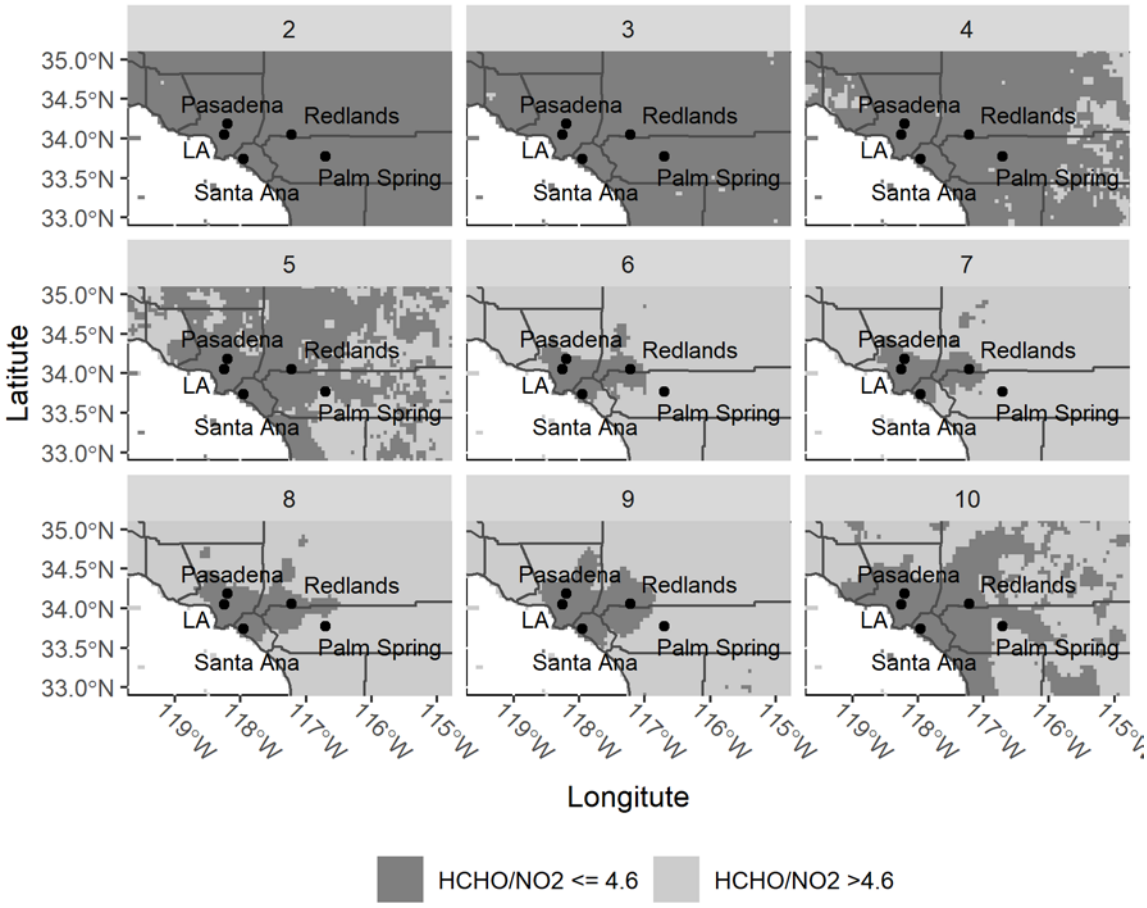

135 **Figure S10. Spatial distribution of O_3 sensitivity regime based on TROPOMI satellite ($HCHO/NO_2$) ratios in Los Angeles for April – October 2020. Light area is in NO_x-limited regime ($HCHO/NO_2 > 4.6$), dark area is in NO_x-saturated regime ($HCHO/NO_2 <= 4.6$)**

11. Sensitivity analysis

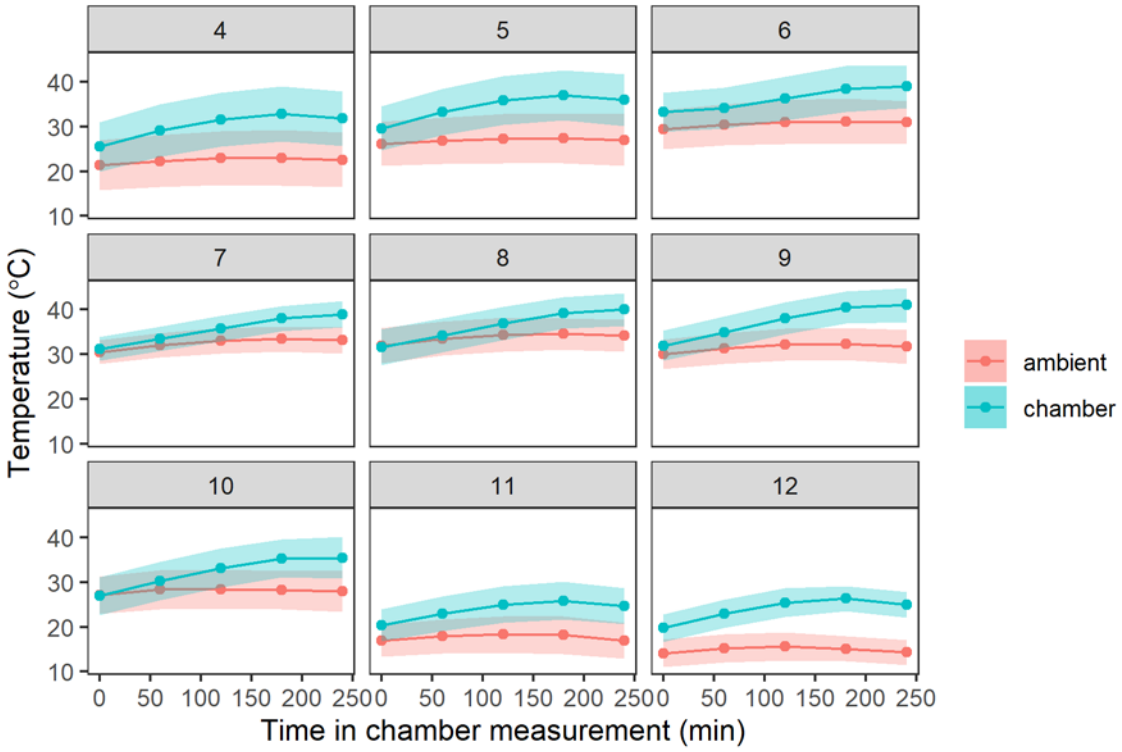

Figure S11. Time series of chamber gas temperature (blue) and ambient temperature (red) for each month from April to December, 2020. The dots show the monthly averaged value, and the shaded area shows the standard deviation of the temperature in each month.

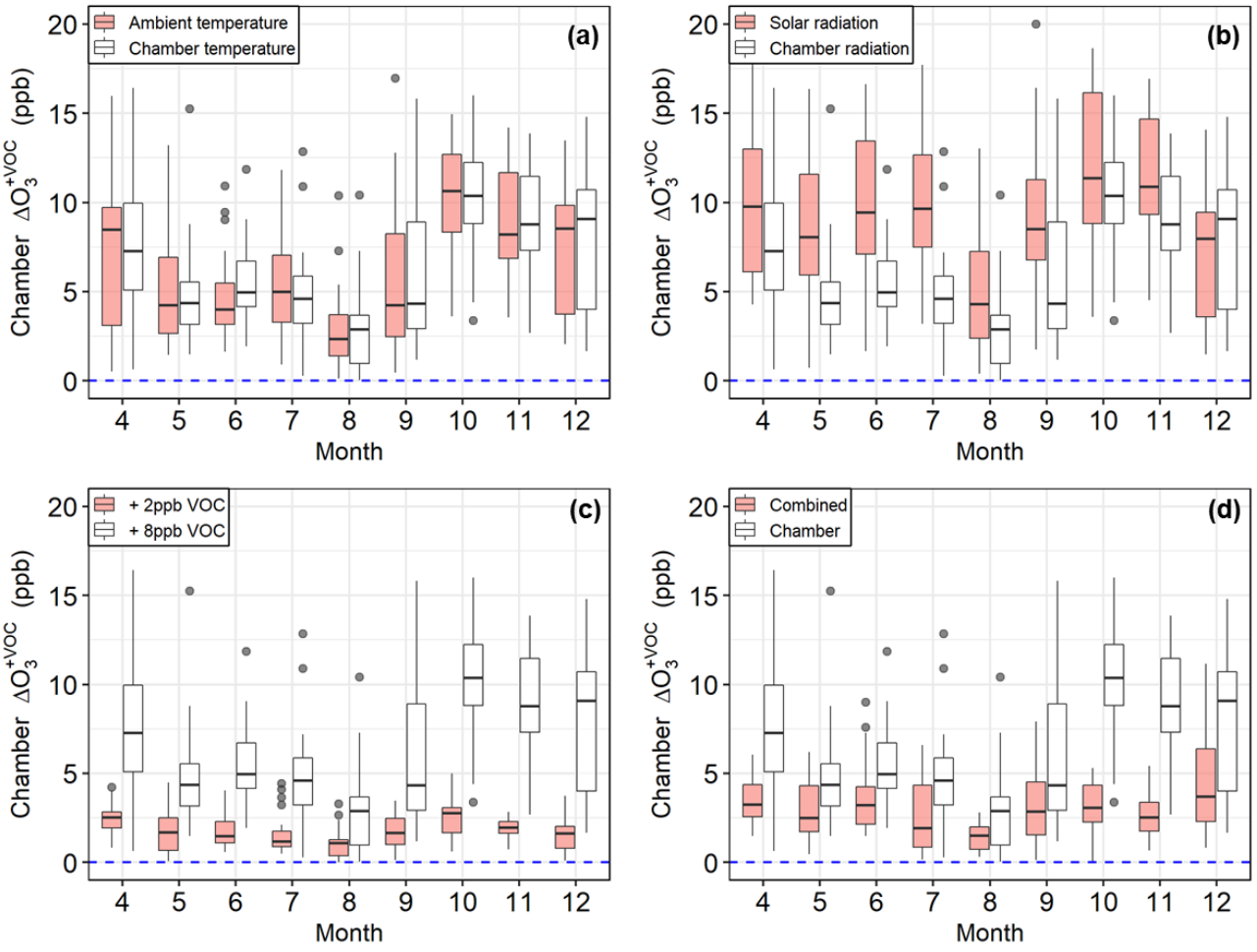

Figure S12. Effect of temperature, radiation, and perturbation amount on the monthly variation of the predicted chamber ΔO_3^{+VOC} from April to December, 2020 at the Sacramento measurement site. Open box constantly shows the calculation under chamber measurement condition (chamber temperature, radiation, and 8ppb VOC perturbation). Solid box reflects the calculation under the change of different condition: (a) under the ambient temperature profile; (b) clear-sky solar radiation; (c) perturbation amount effect: 2 ppb VOC perturbations; (d) the combination of ambient temperature, solar radiation, and 2ppb VOC perturbation.

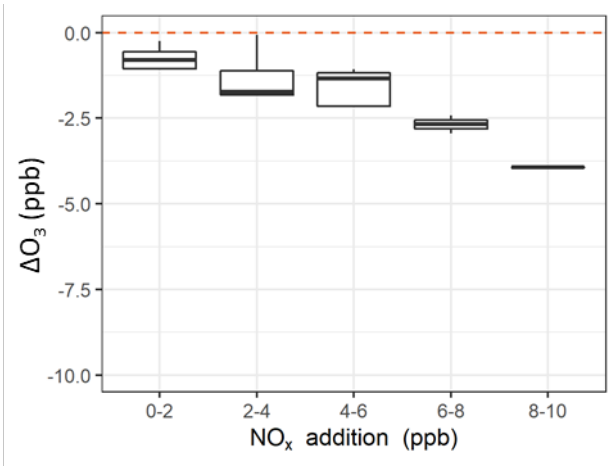

Figure S13. Measured ΔO_3 as a function of different NO_x perturbations. Total number of data points is 24.

155

Reference

Carter, W. P. L. and Heo, G.: Development of revised SAPRC aromatics mechanisms, Atmos. Environ., 77, 404–414, doi:10.1016/J.ATMOSENV.2013.05.021, 2013.

Howard, C. J., Yang, W., Green, P. G., Mitloehner, F., Malkina, I. L., Flocchini, R. G. and Kleeman, M. J.: Direct measurements of the ozone formation potential from dairy cattle emissions using a transportable smog chamber, Atmos. Environ., 42(21), 5267–5277, doi:10.1016/j.atmosenv.2008.02.064, 2008.

Howard, C. J., Kumar, A., Mitloehner, F., Stackhouse, K., Green, P. G., Flocchini, R. G. and Kleeman, M. J.: Direct measurements of the ozone formation potential from livestock and poultry waste emissions, Environ. Sci. Technol., 44(7), 2292–2298, doi:10.1021/es901916b, 2010a.

Howard, C. J., Kumar, A., Malkina, I., Mitloehner, F., Green, P. G., Flocchini, R. G. and Kleeman, M. J.: Reactive organic gas emissions from livestock feed contribute significantly to ozone production in central California, Environ. Sci. Technol., 44(7), 2309–2314, doi:10.1021/es902864u, 2010b.

Venecek, M. A., Cai, C., Kaduwela, A., Avise, J., Carter, W. P. L. and Kleeman, M. J.: Analysis of SAPRC16 chemical mechanism for ambient simulations, Atmos. Environ., 192, 136–150, doi:10.1016/J.ATMOSENV.2018.08.039, 2018.

Ying, Q., Fraser, M. P., Griffin, R. J., Chen, J. and Kleeman, M. J.: Verification of a source-oriented externally mixed air quality model during a severe photochemical smog episode, Atmos. Environ., 41(7), 1521–1538, doi:10.1016/J.ATMOSENV.2006.10.004, 2007.